Cell Reports
Physical Science

CellPress
OPEN ACCESS

Article

A reaction-dissolution strategy for designing solid electrolyte interphases with stable energetics for lithium metal anodes

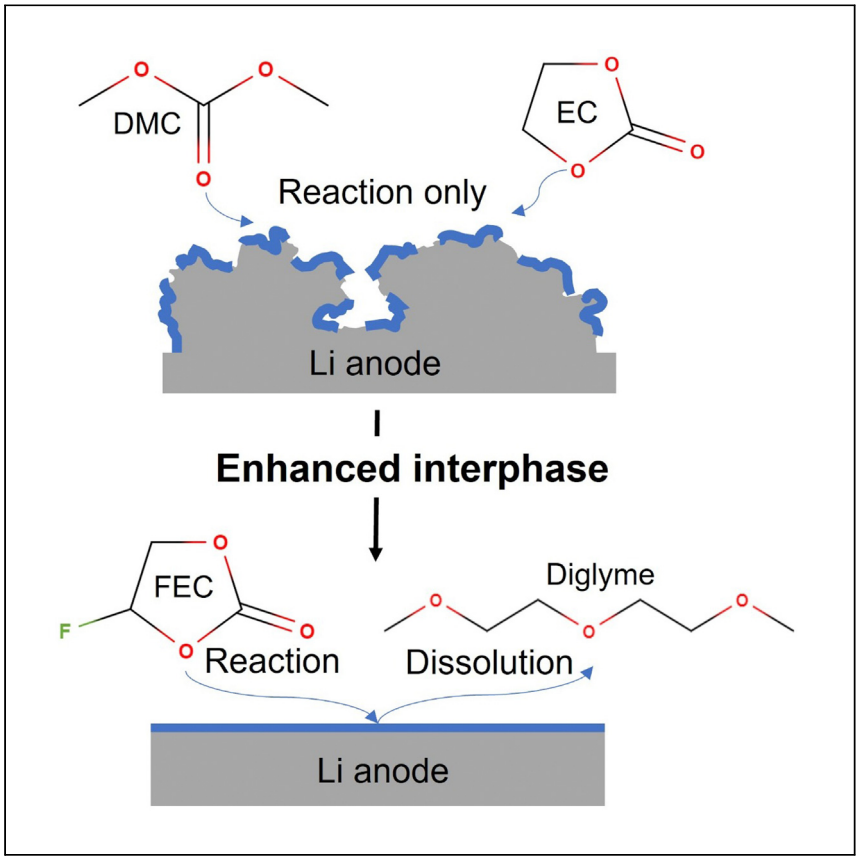

The rechargeability and stability of lithium metal batteries (LMBs) is affected by the interphase between the lithium metal anode and the electrolyte. Biswal et al. report rational selection of liquid electrolyte components to create, refresh, and sustain a kinetically enhanced interphase on the lithium metal anode through the cycle life of LMBs.

Prayag Biswal, Joshua Rodrigues, Atsu Kludze, Yue Deng, Qing Zhao, Jiefu Yin, Lynden A. Archer

laa25@cornell.edu

Highlights

Rational design of liquid carbonate/fluorinated electrolytes with ether additive

Study of physiochemical characteristics and reversibility of metallic lithium (Li)

Employing reaction-dissolution strategy to enhance reversibility of Li anode

Demonstrating practical Li metal batteries with exceptional performance

Biswal et al., Cell Reports Physical Science 3, 100948
July 20, 2022
https://doi.org/10.1016/j.xcrp.2022.100948

Cell Reports
Physical Science

CellPress
OPEN ACCESS

Article

A reaction-dissolution strategy for designing solid electrolyte interphases with stable energetics for lithium metal anodes

Prayag Biswal,[1] Joshua Rodrigues,[1] Atsu Kludze,[1] Yue Deng,[2] Qing Zhao,[1] Jiefu Yin,[1] and Lynden A. Archer[1,2,3,*]

SUMMARY

The spatial variations in chemical composition and transport properties of the interphase formed on reactive metal electrodeposits dictate the stability and reversibility of electrochemical cells that use reactive metals as anodes. Here we report on the influence of carbonate and fluorinated electrolytes infused with ethers as additives on the physical-chemical characteristics and reversibility of metallic lithium (Li) during early stages of electrodeposition and later stages of deep cycling of Li metal anodes. We show that a feasible strategy for achieving and sustaining kinetically enhanced interphases through the cycle life of Li electrodeposits is by simultaneous use of sacrificial electrolyte components that undergo electroreduction to enrich the interphase with fluorinated species in tandem with cleaning electrolyte components that promote dissolution and removal of less desirable carbonaceous compounds. We demonstrate that this approach translates to high electrochemical reversibility during deep cycling of the Li metal anode and improved performance of Li metal batteries.

INTRODUCTION

The spatial variations in chemical composition and transport properties of the solid electrolyte interphase (SEI) formed on lithium (Li) metal in liquid electrolytes are thought to be responsible for the propensity of Li metal electrodes to electrodeposit in irregular, nonplanar morphologies during repeated charge/discharge cycles.[1] The origin of these spatial variations is thought to be parasitic reactions of Li with electrolyte components (solvent, salt, and additives), forming a spectrum of inorganic and organic products (i.e., Li_2CO_3, LiF, LiOH, Li_2O, LiH, and ROLi and $ROCO_2Li$ class oligomers) at the interface.[1,2] A chemically inhomogeneous SEI means that ion transport and mechanics vary from location to location on Li, which is thought to favor Li electrodeposition at specific points during charging.[3] The nascent deposits formed serve as centers of concentrated electric field lines of incoming Li ions, directing the electrodeposition thereon, and grow disproportionately to micrometer size in a short period of time.[4,5] As these deposits grow, they break through the inherent SEI, further reacting with the electrolyte to form a fresh SEI composed of decomposition products. During the discharging phase, these spatial variations in the SEI enable non-uniform local dissolution of Li from the electrode, leading to pitting of the electrode and further collapse of the SEI because of pits formed in the process.[5,6] This process is exacerbated by repeated charge/discharge cycles of the metal electrode, leading to mechanical loss of active metal and chemical loss of electrolyte components and deteriorating electrochemical

[1]Robert Frederick Smith School of Chemical and Biomolecular Engineering, Cornell University, Ithaca, NY 14853, USA

[2]Department of Materials Science and Engineering, Cornell University, Ithaca, NY 14853, USA

[3]Lead contact

*Correspondence: laa25@cornell.edu

https://doi.org/10.1016/j.xcrp.2022.100948

reversibility of a Li metal battery. The continuous reaction of the electrodeposited Li with the electrolyte throughout the cycles results in a thicker SEI and lower interfacial ionic conductivity relative to the electrolyte bulk, which increases polarization and accelerates decomposition of the electrolyte.[7]

A growing body of work reports that selectively modifying the chemistry and transport properties of the SEI by incorporating certain additives in liquid electrolytes is an effective approach for achieving highly reversible Li electrodeposition in liquid electrolytes.[8–16] Equilibrium theoretical calculations using joint density functional analysis in a vacuum and generic liquid (e.g., acetonitrile) medium have also shown that in-plane transport at such interphases is enhanced substantially when LiX (X = Br > Cl > F) species are the only components of the SEI.[17] Previous work builds on this hypothesis to investigate whether deliberate incorporation of these halide (F, Br) species into the SEI via partially fluorinated/brominated electrolytes affects the early-stage growth and reversibility of Li electrodeposits.[4,18] The results show improvement in the surface energetics (ion diffusivity, interfacial energy) of the SEI and also indicate that Li electrodeposits with a more uniform morphology form in the early stages of electrodeposition. However, the improvements in the reversibility of the electrodeposits observed during long-term, deep cycling of Li are modest at best compared with conventional carbonate electrolytes. We hypothesize that the failure to realize deep cycling of the Li anode in halide-enriched electrolytes stems from at least three reasons. First, conventional carbonate electrolyte, which serves as the carrier medium for halide-rich additives, actively decomposes into carbonaceous compounds (Li_2CO_3, $ROCO_2Li$, etc.) at the reducing potentials (−3.04V versus standard hydrogen electrode) at which Li^+ reduces to form Li at the anode during battery charging. Second, the formed carbonate compounds that ultimately dominate the composition of the SEI fundamentally alter the interfacial ion transport properties, negating any benefits of the fluorinated components. To demonstrate this point more concretely, a purely Li_2CO_3-rich SEI has an about five times higher energy barrier for diffusion of in-plane Li adatoms than a purely LiF SEI.[17] Similarly, the ion diffusion properties of the SEI are also hindered by the presence of Li_2CO_3.[4,18] Repeated plating/stripping cycles of the anode generate a significant amount of these compounds at the SEI in the long run, which negates any beneficial effects of the halide additives in the early stage. Finally, mitigating the parasitic reactions and preserving the halide-rich SEI over repeated plating/stripping cycles of the Li anode provides a strategy for realizing high electrochemical reversibility for deep cycled Li.

An approach to reduce the parasitic reactions at the interphase is to substitute the conventional carbonate electrolyte with a fully fluorinated electrolyte. This can be realized by adding large amounts of easily reduced fluorine-rich salts (e.g., $LiPF_6$, LiFSI) into the conventional carbonate or ether-based solvents (e.g., ethylene carbonate/dimethyl carbonate or dimethyl ether/dioxolane) to create a highly concentrated electrolyte where the salt dominates over the solvent in regulating the SEI[9,10,19,20] or by simply replacing the base solvent with a fluorinated analog (fluoroethylene carbonate).[10] The latter approach is studied here because it is considered more feasible; the high cost of salt in a highly concentrated electrolyte can easily outweigh any potential benefit of a Li metal anode.[20] Fluoroethylene Carbonate (FEC) is selected here because it is often employed as an electrolyte additive because of its reported beneficial influence on the morphology of Li electrodeposits formed in charge/discharge battery cycling experiments.[10,16,21] FEC regulates the solvation sheath of Li ions to promote preferential reduction, which actively passivates the anode with a fluorine-rich SEI layer.[22,23] We have shown previously that

carbonate electrolytes containing FEC as an additive, even in low weight percentages (~10 wt %), yield a more uniform plating morphology of Li.[4] By means of X-ray photoelectron spectroscopy (XPS) analysis, this behavior was attributed to FEC's ability to form a fluorine-rich SEI. FEC is also expected to serve a dual-purpose role of stabilizing the Li anode imparted by LiF-rich SEI formation and enhancing oxidative stability of the electrolyte.[10,24] Recently, its role as a single component electrolyte solvent in enabling highly reversible 5V class Li metal batteries has garnered attention.[10] Although FEC can stabilize the SEI, realizing elimination of any parasitic side reactions and unwanted side products over hundreds of charge/discharge cycles of the anode is a requirement for progress toward practically relevant Li metal batteries. Specifically, FEC, a fluorinated carbonic ester with structural similarity to that of conventional carbonate solvents (ethylene carbonate), is expected to generate carbonaceous compounds (Li_2CO_3, $ROCO_2Li$) as side products. This means that the beneficial fluoride-enriched interphase formed in the early stages of Li deposition can be easily overwhelmed by carbonates. The fluoride-rich interface can, however, be sustained via a solubilizing/cleaning agent capable of dissolving the side products from the SEI. Cleaning agents of choice can be glycol ethers (glymes), a group of saturated non-cyclic polyethers commonly used in paints and cleaners for precisely that purpose.[25]

We investigate the physicochemical characteristics and electrochemical reversibility of metallic Li in carbonate and fluorinated electrolytes with or without glymes. Electrodeposition of Li is carried out across a set of carbonate (ethylene carbonate [EC]:dimethyl carbonate [DMC]) and fluorinated (FEC) electrolyte chemistries incorporated with a glyme additive (diglyme [G2]): 1M $LiPF_6$ in EC:DMC (50:50), 1M $LiPF_6$ in EC:DMC:G2 (45:45:10), 1M $LiPF_6$ in FEC, and 1M $LiPF_6$ in FEC:G2 (90:10). We hypothesize that regulation and preservation of the surface energetics of the SEI through the cycle life of Li electrodeposits is crucial for achieving high reversibility, and this is feasible through the SEI fluorine enrichment mechanism of FEC in tandem with the cleaning action of the G2. The spatial and chemical characteristics of electrodeposited Li are studied via a combination of scanning electron microscopy (SEM), energy-dispersive X-ray (EDX), XPS, and electrochemical impedance spectroscopy (EIS) techniques. Consistent with our previous report,[4] we show that fluorine-enriched SEI is spatially homogeneous and has favorable kinetics for uniform Li deposition in early stages of electrodeposition. We also show that the glyme additive (G2), even in modest proportions, can solubilize the unwanted carbonaceous compounds and preserve the pristine fluorine-enriched SEI for later cycles, enabling higher reversibility, longer cycle life, and decidedly nondendritic morphology for the Li metal anode. Cycling studies in electrochemical cells composed of thin metallic Li anodes (50 μm) and commercial-grade nickel cobalt manganese oxide (NCM) cathodes reveals that a fluorinated electrolyte with a glyme additive enables high Coulombic efficiency (CE) and stable long-term cell operations.

RESULTS AND DISCUSSION

Physicochemical characterization of nascent SEI

The SEI was formed via galvanostatic polarization of bulk electrolyte onto a heterogeneous surface composed of polished stainless steel (SS; average roughness, 9.12 ± 8.78 nm). To investigate the effect of fluorinated electrolytes (FEC) and the glyme additive (G2) on the spatial homogeneity of the interphase, the SEI was formed from electrolytes of different compositions (1M $LiPF_6$ in EC:DMC [50:50], 1M $LiPF_6$ in EC:DMC:G2 [45:45:10], 1M $LiPF_6$ in FEC, and 1M $LiPF_6$ in FEC:G2 [90:10]) by discharging the Li on polished SS (Li||SS) cell at current density of 0.5 mA/cm^2 until the potential

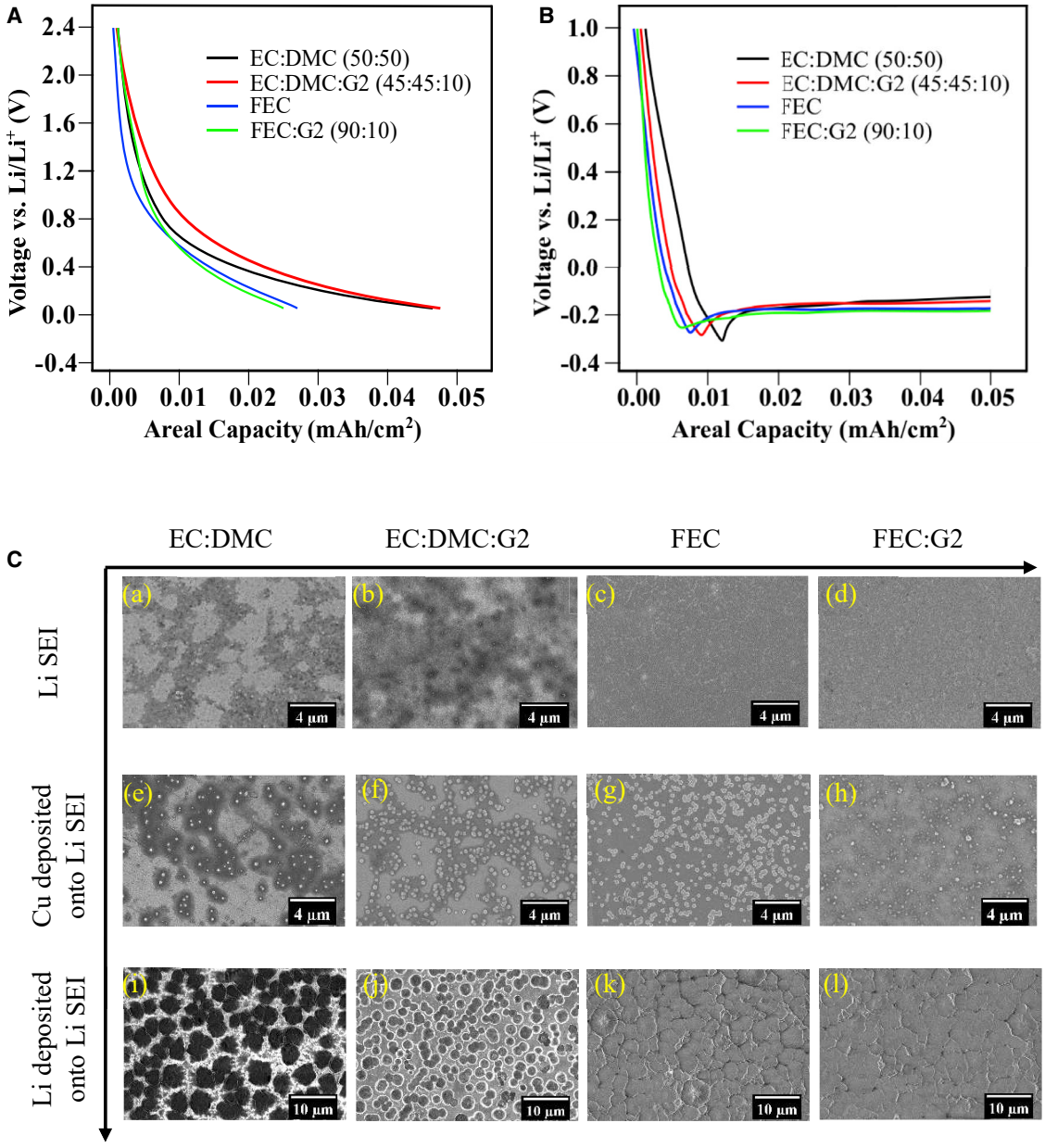

Figure 1. Effect of electrolyte chemistry on the morphology and homogeneity of early-stage SEI and electrodeposits of Li formed on polished SS

(A) Experimental voltage profiles of galvanostatic SEI formation for different electrolyte compositions at a current density of 0.5 mA/cm^2.

(B) Experimental voltage profiles of Li electrodeposition from electrolyte of different compositions at a current density of 1 mA/cm^2 and capacity of 0.05 mAh/cm^2.

(C) *Ex situ* SEM images captured of (a–d) Li SEI formed galvanostatically at 0.5 mA/cm^2, (e–h) Cu deposited at a current density of 1 mA/cm^2 and capacity of 0.01 mAh/cm^2 onto the previously formed Li SEI in different electrolytes, and (i–l) Li deposited at a current density of 1 mA/cm^2 and capacities of 0.05 mAh/cm^2 onto the previously formed Li SEI for the range of electrolyte compositions. The electrolyte compositions are 1M $LiPF_6$ in EC:DMC (50:50), 1M $LiPF_6$ in EC:DMC:G2 (45:45:10), 1M $LiPF_6$ in FEC, and 1M $LiPF_6$ in FEC:G2 (90:10). The Li is deposited from the above electrolytes for the corresponding SEI, whereas copper is deposited from 0.5M $Cu(OTF)_2$ in EC:DMC (50:50) electrolyte in all cases. All ratios are volume percent. G2, diglyme.

dropped to 50 mV versus Li^+/Li, as shown in Figure 1A. The terminal discharge potential of 50 mV was chosen to avoid any substantial underpotential deposition of Li, which is likely at around 0 V. Then the cell was galvanostatically charged back to 1.5 V at low currents of 0.1 mA/cm^2 to strip the underpotentially deposited Li, if any. The areal

capacity of SEI formation decreased almost 2-fold between the carbonate electrolyte and the fluorinated electrolyte (i.e., 0.047 mAh/cm^2 for EC:DMC compared with 0.027 mAh/cm^2 for FEC), as shown in Figure 1A. Both electrolytes are known to actively reduce at potentials above 0 V to form products that can electronically passivate the SS.[22,26,27] This capacity is a measurable indicator of the amount of electrolyte reduced at a fixed current to form the SEI on the SS. This formation step, occurring over a range of potentials, involves competing reactions, which often results in several side products. The lower capacity observed in formation of the SEI for the fluorinated electrolyte suggests fewer side reactions and quicker electronic passivation of the heterogeneous surface than the carbonate electrolyte. No change in areal capacity was observed between the base electrolytes and G2-infused variants (i.e., EC:DMC versus EC:DMC:G2 and FEC versus FEC:G2), indicating that the G2 acts as inert to decomposition in SEI formation because of its low reduction potential against Li (calculated to be between −0.8 and −0.2 V versus Li$^+$/Li)[28] and significantly lower proportion in the electrolyte mixtures.

The morphological features of the SEI formed across the range of electrolytes were mapped using SEM, as shown in Figure 1C (a–d). The observed SEI for carbonate electrolytes (Figure 1C [a and b]) has spatial regions of different contrast as opposed to the uniform contrast observed in fluorinated electrolytes (Figure 1C [c and d]). Point spectrum chemical analysis of these regions performed via EDX in tandem with the SEM shown in Figure S1 (A–D) and quantified in Table S1A indicates the darker contrasted regions to be rich in fluorine as opposed to the lighter regions having higher carbon weight percentage. The degree of spatial contrast is highest in the case of base carbonate electrolyte (Figures 1C [a] and S1A), suggesting that the SEI formed in this electrolyte is spatially inhomogeneous with alternating fluorine and carbon-rich regions. As an example, in Figure S1A, the darker contrasted region a1 has F and C weight percentages of 54.2 and 35.7, respectively, compared with 24.1 and 69.2, respectively, in the lighter contrasted region a2. This is due to the fact that, during the electrolyte reduction, the electrolyte components decompose at different potentials to form different products; i.e., $LiPF_6$ decomposes at more positive potentials[26,27] to form fluorine-rich products (LiF), whereas the solvent EC:DMC decomposes at more negative potentials[26,27] to form carbon-rich products (Li_2CO_3, $ROCO_2Li$, etc.).[1] As these products precipitate at the interface, they electronically passivate it, resulting in a patchy SEI. Addition of the G2 to the base carbonate electrolyte seems to rectify the patchy SEI. The SEI has less of a spatial contrast in morphology and more fluorine-rich regions (darker contrast), as shown in Figure 1C (b) and analyzed in Figure S1B. This is most likely due to the hypothesized solubilizing action of G2 on carbon-rich precipitates at the interface. The SEI formed in fluorinated electrolytes (FEC and FEC:G2) is rich in fluorine content and lacks any spatial contrast; i.e., it is homogeneously fluorine rich all across the surface, as shown in Figure 1C (c and d) and analyzed in Figure S1 (C and D). The higher degree of uniformity is crude because both $LiPF_6$ and FEC form LiF as a major product during decomposition.

The SEI-covered SS substrates are harvested and studied via deposition of Cu onto them from a carbonate electrolyte. The aim is to contrast the ionic transport properties of the spatial regions of the SEIs by analyzing the deposition patterns of a non-reactive metal like Cu. Cu is galvanostatically electrodeposited onto the SEI from 0.5M $Cu(OTF)_2$ in EC:DMC (50:50) electrolyte at current density of 1 mA/cm^2 and capacity of 0.01 mAh/cm^2. The capacity of electrodeposition is deliberately kept low to avoid any modification of the inherent SEI. The potentials of electrodeposition recorded are in the range of 2–2.2 V versus Li$^+$/Li, which is well above the

Please cite this article in press as: Biswal et al., A reaction-dissolution strategy for designing solid electrolyte interphases with stable energetics for lithium metal anodes, Cell Reports Physical Science (2022), https://doi.org/10.1016/j.xcrp.2022.100948

reduction potential of the carbonate solvent (0.5M $Cu(OTF)_2$ in EC:DMC [50:50]) employed,[26,27] indicating minimal decomposition of the new electrolyte and, hence, reduced interference with the previously formed SEIs. Figure 1C (e–h) shows the morphology of the Cu electrodeposits on the previously formed SEIs. The chemistry of these morphological features is further analyzed in Figure S1 (E–H) and Table S1B. Quite like before, the darker contrasted regions are fluorine rich, whereas the lighter contrasted regions are carbon rich; also, the spatial and chemical contrast is more vivid in the base carbonate electrolyte (Figures 1C [e] and S1E); e.g., in Figure S1E, the darker contrasted region e1 is fluorine rich (F, 53.9 wt %; C, 8.7 wt %), the lighter contrasted region e2 is carbon rich (F, 28.6 wt %; C, 69.8 wt %), and the Cu deposit region e3 is Cu rich (Cu, 83.4 wt %; F, 8.4 wt %; C, 6.0 wt %). The proximity and overlap of the Cu deposit region e3 with fluorine-rich region e1 suggests that Cu ions preferentially diffuse across the fluorine-rich spots and charge transfers to form Cu deposits. This is apparent across the entire set of electrolyte chemistries studied, as shown in Figure 1C (e–h) and analyzed in Figure S1 (E–H). In the case of the SEI formed by fluorinated electrolytes (Figures 1C [g and h] and S1 [G and H]), the Cu deposits are well distributed across the surface. It can be speculated that the fluorine-rich regions have a lower energy barrier to ion transport, enabling metal transport and reduction through them. Enhancing the coverage of the surface by the fluorine-rich regions can enable uniform and facile nucleation of metal.

Physicochemical characterization of nascent Li electrodeposits

The SEI-covered substrates were subjected to galvanostatic deposition of metallic Li from the corresponding set of electrolytes at a current density of 1 mA/cm^2 and capacity of 0.05 mAh/cm^2. The small areal capacity is equivalent to an electrodeposit film thickness of 300 nm when Li electrodeposits have the same density as bulk Li metal. The voltage response profiles are shown in Figure 1B, and *ex situ* postmortem analyses of the substrates are shown in Figure 1C (i–l). The overpotential curves (voltage response curves) across all electrolytes show the typical behavior of a voltage dip because of any remnant SEI formation, a voltage peak at about a capacity of 0.006–0.012 mAh/cm^2 because of metal nucleation, and voltage plateauing because of subsequent electroplating of ions onto the nuclei in the growth phase.[4] The areal capacity and overpotential at metal nucleation vary with electrolyte composition (0.012, 0.009, 0.008, and 0.066 mAh/cm^2 and 0.31, 0.29, 0.28, and 0.25 V for EC:DMC, EC:DMC:G2, FEC, and FEC:G2 respectively); i.e., both values are lower for the fluorinated electrolyte than the carbonate electrolyte, and addition of G2 further diminishes them. The decrease in areal capacity and overpotential of nucleation across the electrolytes suggests that a facile SEI is enabling lower diffusion and charge transfer energy barrier for electrodeposition of the Li ions. A significant change in morphology of electrodeposits is also observed across the electrolytes, as apparent in Figure 1C (i–l). The carbonate electrolyte (EC:DMC) forms distinct three-dimensional (3D) spherical structures with a radius of 1.8 μm on the SS substrate (Figure 1C [i]). Addition of G2 diminishes the sizes to 1.1 μm and increases the areal density of these electrodeposits (Figure 1C [j]), most likely because of an increase in spatial homogeneity of the SEI, as observed previously. This can be rationalized as follows. The G2 added carbonate electrolyte (EC:DMC:G2) forms a more spatially homogeneous SEI than the base carbonate electrolyte (EC:DMC), as shown in Figure 1C (a and b). A spatially homogeneous SEI imparts a higher number of nucleation points for the incoming Li ions, thereby forming a higher number of smaller nuclei all over the surface for equal capacities of electrodeposition. This effect of spatial homogeneity on the morphology of Li electrodeposits is even more apparent in the case of fluorinated electrolytes (FEC, FEC:G2), as shown in Figure 1C (k and l). The electrodeposits are planar (2D), film-like, and entirely cover the surface, making the bright SS background virtually invisible.

Please cite this article in press as: Biswal et al., A reaction-dissolution strategy for designing solid electrolyte interphases with stable energetics for lithium metal anodes, Cell Reports Physical Science (2022), https://doi.org/10.1016/j.xcrp.2022.100948

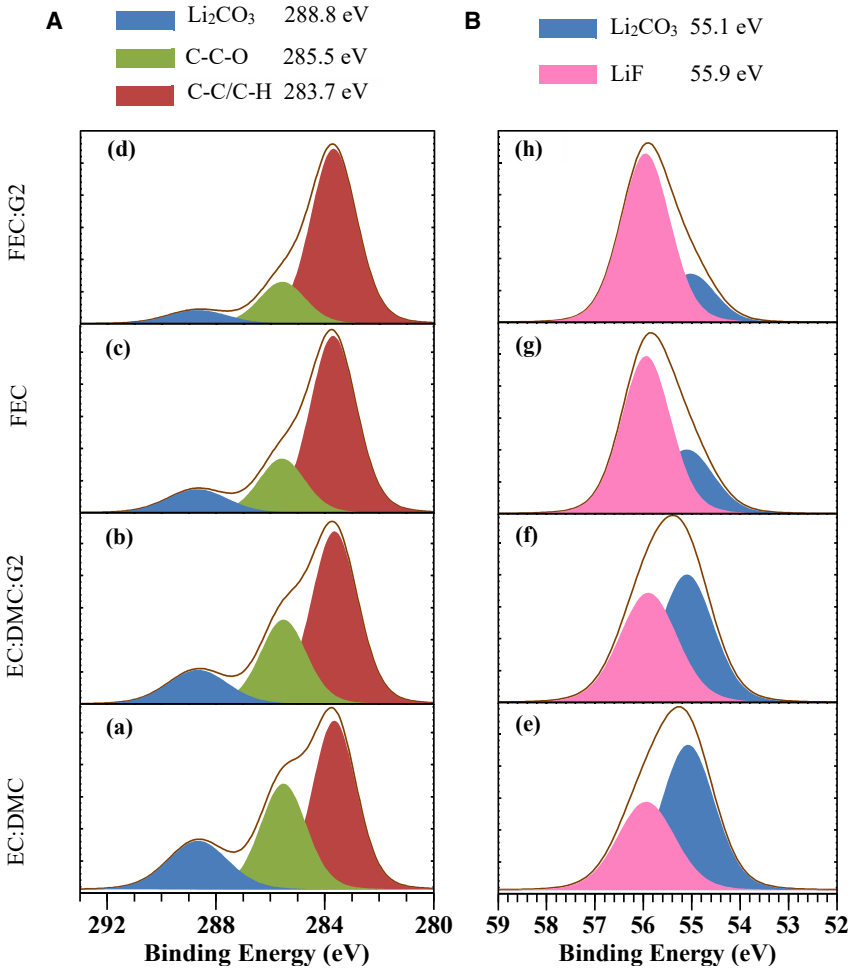

Figure 2. Interfacial chemistry of Li electrodeposits formed at low capacity

(A and B) (A) C 1s and (B) Li 1s high-resolution spectra of the SEI layer on Li electrodeposits formed at a current density of 1 mA/cm^2 for an areal capacity of 0.05 mAh/cm^2 from electrolytes of different compositions: (a and e) EC:DMC (50:50), (b and f) EC:DMC:G2 (45:45:10), (c and g) FEC, and (d and h) FEC:G2 (90:10), each containing 1M $LiPF_6$ salt.

To identify root causes for our observations, XPS was performed to investigate the surface chemistry of SEIs formed in the early stages of Li electrodeposition (i.e., a capacity of 0.05 mAh/cm^2) across the set of electrolyte chemistries being studied. The results are reported in Figures 2 and S2A, Tables S2A and S3A. Distinct changes in the chemical composition of the SEI can be readily observed. The survey spectrum in Figure S2A shows multiple atomic peaks, of which Li 1s (55.5 eV), carbon 1s (284.5 eV), oxygen 1s (531.6 eV), phosphorous 2p (133 eV), and fluorine 1s (684.9 eV) are relevant. The atom percentage of fluorine increases, and the atom percentages of carbon and oxygen decrease across the electrolyte chemistries. The fluorinated electrolytes (FEC, FEC:DG) show a higher percentage of fluorine and lower percentage of carbon and oxygen than the carbonate electrolytes (EC:DMC, EC:DMC:G2); e.g. the SEI of FEC has F (28.46%), C (19.96%), and O (12.55%) compared with F (20.1%), C (29.96%), and O (22%) of EC:DMC. Electrolytes with G2 additives show a similar trend in atom percentages of fluorine, carbon, and oxygen when contrasted with their counterparts (without G2 additive); e.g. the SEI of EC:DMC:G2 has F (24.61%), C (23.02%), and O (12.98%) compared with F (20.1%), C (29.96%), and

O (22%) of EC:DMC. The fluorine-to-carbon and fluorine-to-oxygen ratios increase about 2-fold and 3-fold, respectively, when comparing the G2-added fluorinated electrolyte (FEC:G2) with the base carbonate electrolyte (EC:DMC).

A closer look at the high-resolution spectra of carbon and Li is necessary to better understand the nature of bonding between carbon, oxygen, fluorine, and Li in the SEI that might prompt these observations. Figure 2 shows the high-resolution spectra of carbon (C 1s) and Li (Li 1s) in the SEI, and the results are tabulated in Tables S2A and S3A. There are three distinct peaks in the C 1s spectra: Li_2CO_3 at 288.8 eV, C-C-O at 285.5 eV, and C-C/C-H at 283.7 eV (Figure 2A). The Li_2CO_3 and C-C-O peaks are diminished and the C-C/C-H peak is enhanced across the set of electrolyte chemistries; e.g., when comparing the two ends of the electrolyte spectrum, EC:DMC has 19.17% Li_2CO_3, 32.12% C-C-O, and 48.62% C-C/C-H compared with 7.66% Li_2CO_3, 17.89% C-C-O, and 74.45% C-C/C-H of FEC:G2 (Table S2A). Also, there are two distinct peaks in the Li 1s spectra: Li_2CO_3 at 55.1 eV and LiF at 55.9 eV (Figure 2B). The 55.1-eV region of the Li 1s spectrum is superimposed with Li_2CO_3, LiOH, and Li2O, with Li_2CO_3 being the major inorganic product because of decomposition of the carbonate-based electrolytes. Therefore, the compositions inferred from this region are approximate. The LiF peak is enhanced and the Li_2CO_3 peak is diminished across the set of electrolyte chemistries studied; e.g., when comparing the two ends of the electrolyte spectrum again, EC:DMC has ~60.42% Li_2CO_3, and 39.58% LiF compared with ~22.42% Li_2CO_3, and 77.58% LiF of FEC:G2 (Table S3A). The above observations can be rationalized as follows. The fluorinated electrolyte (FEC) decomposes to form LiF and oxygen-free ethylene species (C-C) as major products, which may electropolymerize at the reducing anode potentials to form a fluorinated SEI enriched in polyene (-C-C-) networks. The SEI formed is deficient in carbonates, polyethers, and alkoxides (e.g., Li_2CO_3, $ROCO_2Li$, ROLi, $-CH_2O-$), like oxygen-rich species. This observation is consistent with previous reports.[29–31] The G2 additive, being a polyether (C-C-O), solubilizes the oxygen-rich carbon species (e.g., Li_2CO_3 and ethylene oxide [C-C-O]-rich species) but does not affect the polyene species (-C-C-) in the SEI, enhancing the fluorine and ethylene content of the SEI. The principle of solubility here is based on "like dissolves like"; e.g., Li_2CO_3 is determined to be about 10 times more soluble than LiF in G2, as shown in Figure S3B. Therefore, the SEI formed in FEC:G2 is observed to have the highest percentage enrichment in fluorine and ethylene linkages across the electrolyte chemistries studied.

EIS and fast cyclic voltammetry performed on the Li electrodeposits formed at low capacities (0.05 mAh/cm^2) on SS reveals transport and reaction characteristics of Li ions in the SEI, as shown in Figures 3 and S4. All Nyquist plots (Figure 3A) show a depressed semi-circle with a Warburg region, which can be fitted to the model in Figure S4A, and the extracted data are plotted in Figure S4B. The characteristic frequencies a', b', and c' of the Nyquist plots are shown in Table S4. The fluorinated electrolyte (FEC) shows lower SEI and charge transfer (CT) resistance than the carbonate electrolytes (EC:DMC). The addition of G2 additive to these electrolytes further lowers the resistance, with the interphase formed in FEC:G2 having the lowest resistance of all; i.e., FEC:G2 (98.4 Ω/cm^2 [SEI], 450.5 Ω/cm^2 [CT]) has an almost 2-fold lower resistance compared with EC:DMC (158.7 Ω/cm^2 [SEI], 82.6 Ω/cm^2 [CT]). Further, the ion diffusivity (*Ds*) of the SEI, determined from the Warburg region, is shown in Figure 3C. The result indicates that *Ds* increases 4-fold across the set of electrolyte chemistries; the *Ds* values are as follows: 1.19×10^{-17} m^2/s (EC:DMC), 3.02×10^{-17} m^2/s (EC:DMC:G2), 3.29×10^{-17} m^2/s (FEC), and 4.7×10^{-17} m^2/s (FEC:G2). Enriching the SEI formed in carbonate electrolytes

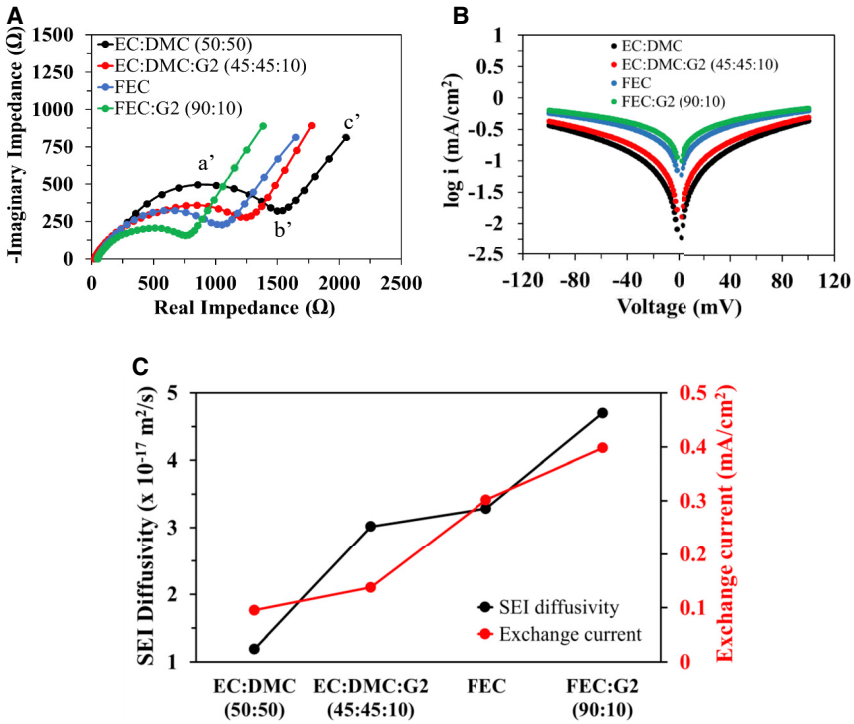

Figure 3. Interfacial transport and reaction kinetics of Li electrodeposits formed on SS in electrolytes of different chemistries at a current density of 1 mA/cm^2 and low capacity of 0.05 mAh/cm^2

(A) Impedance plots (Nyquist) of Li electrodeposits obtained via EIS. a', b', and c' represent the frequency at the apex of the depressed semi-circle, at the turning point between the semi-circle and the Warburg tail, and at the endpoint of the Warburg tail, respectively.

(B) Tafel plots for electrodeposited Li obtained via fast scan cyclic voltammetry (CV) (i.e., 100 mV/s in the range 100 mV to –100 mV). The exchange current and charge transfer (CT) coefficient are calculated by fitting linear regions of the plots (i.e., –80–40 mV and 40–80 mV).

(C) Plot of SEI *Ds* (as extracted from impedance plots) and i_o (as extracted from Tafel plots). The electrolytes are EC:DMC (50:50), EC:DMC:G2 (45:45:10), FEC, and FEC:G2 (90:10), each containing 1M $LiPF_6$ salt.

with fluorine via an FEC additive is known to enhance Li *Ds*.[4] Recent modeling studies have also shown the SEI diffusivity[32–34] to be anywhere between 10^{-16} and 10^{-26} m^2/s, with higher values ($\sim 10^{-16}$ m^2/s) reported for a purely LiF interface. Fast scan CV performed to probe the reaction kinetics of the SEI shows a similar trend in exchange current density (i_o) of the electrolytes (Figures 3B and 3C). The CT coefficient (α) is shown in Table S5. The i_o increases about 4-fold across the electrolyte spectrum: 0.09 mA/cm^2 (EC:DMC), 0.14 mA/cm^2 (EC:DMC:G2), 0.30 mA/cm^2 (FEC), and 0.39 mA/cm^2 (FEC:G2). These measurements are in accord with the observed lowering of nucleation overpotential (Figure 1B) and SEI and CT resistance (Figure S4B) because increased *Ds* and i_o suggest facile transport and reduction of Li^+ at the interface. A higher surface diffusivity indicates relatively easier 2D migration of Li ions in the fluorinated SEI, promoting more spread out/delocalized electrodeposition, as shown in Figure 1C (k and l).

This analysis provides insights into the roles of surface homogeneity, chemistry, and energetics in uniform plating of Li at low capacity. However, it remains to be determined whether the surface energetics, chemical nature, and uniform morphology observed at low capacities translate to a similar morphology and energetics at later

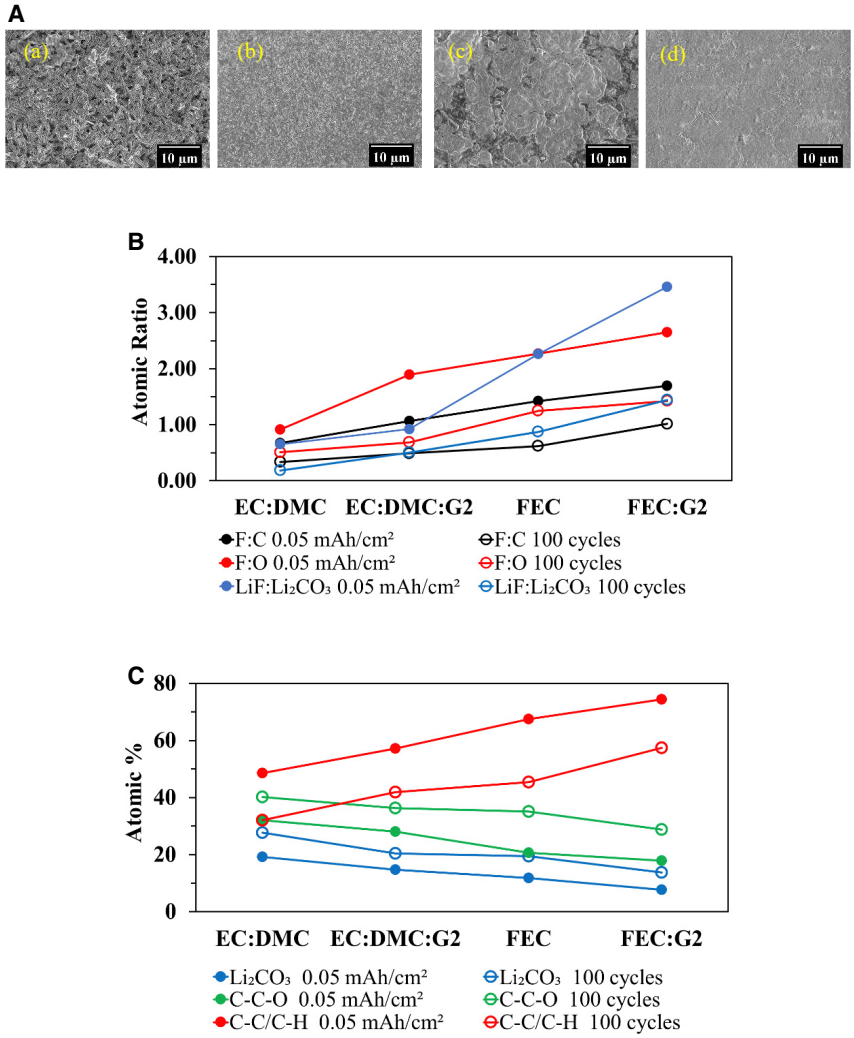

Figure 4. Effect of electrolyte chemistry on the morphology and interfacial chemistry of Li electrodeposits on SS substrate after 100 plating/stripping cycles at 1 mA/cm^2 and 1 mAh/cm^2

(A) *Ex situ* SEM images of the electrodeposited Li morphology after 100 cycles for different electrolytes: (a) EC:DMC (50:50), (b) EC:DMC:G2 (45:45:10), (c) FEC, and (d) FEC:G2 (90:10).

(B) Plot of the atomic ratio of fluorine to carbon, fluorine to oxygen, and Li fluoride to Li carbonate of the SEI formed at 0.05 mAh/cm^2 and after 100 cycles for different electrolytes.

(C) Plot of atomic percentage of components of carbon 1s high-resolution spectra of the SEI formed at 0.05 mAh/cm^2 and after 100 cycles for different electrolytes. Each of the electrolytes contains 1M $LiPF_6$ salt.

stages of charge/discharge cycling at higher capacity relevant for applications in practical Li metal batteries (LMBs). In this context, we study the morphology, chemical composition, and surface energetics of electrodeposited Li after several plating/stripping cycles (Figures 4 and 5). We further investigate the electrochemical reversibility of Li electrodeposits via CE and galvanostatic plating/stripping of symmetric Li cells (Figure 6). Finally, the electrochemical performance of full cells containing thin Li metal (~50 μm) paired against an NCM cathode with the electrolytes is evaluated (Figure 7).

Physicochemical characterization of post-cycled Li electrodeposits

Li was galvanostatically plated/stripped for 100 cycles onto a polished stainless substrate at current density of 1 mA/cm^2 from liquid electrolytes of different

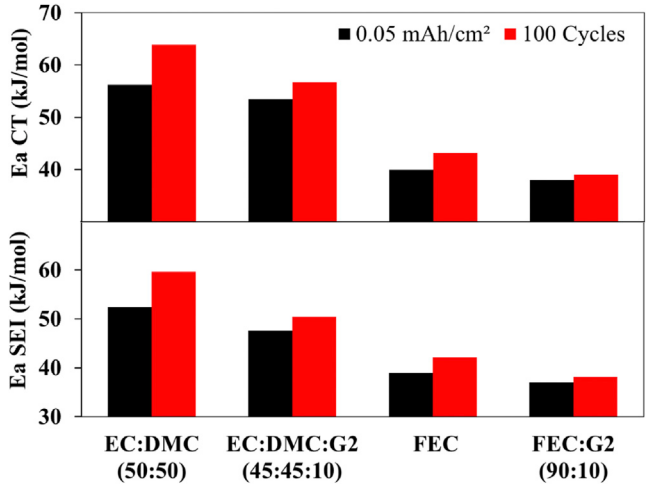

Figure 5. Effect of electrolyte chemistry on the activation energies (SEI and CT) of the interphase of Li electrodeposits on SS substrate at 0.05 mAh/cm^2 and after 100 plating/stripping cycles at 1 mA/cm^2 and 1 mAh/cm^2

The electrolytes are EC:DMC (50:50), EC:DMC:G2 (45:45:10), FEC, and FEC:G2 (90:10), each containing 1M $LiPF_6$ salt. The activation energies are obtained through Arrhenius fitting of SEI and CT resistances at different temperatures.

compositions for a higher capacity of 1 mAh/cm^2; i.e., about an order of magnitude higher than the low capacity of 0.05 mAh/cm^2. Figure 4A shows a panel of *ex situ* SEM images of the electrodeposits. The morphology of Li electrodeposits is entwined wire-like mossy dendrites for EC:DMC (Figure 4A [a]), in contrast with the relatively smooth morphology of EC:DMC:G2 (Figure 4A [b]). Similar contrasting observations were made for FEC (Figure 4A [c]) and FEC:G2 (Figure 4A [d]); i.e., the FEC:G2 case has a more uniform morphology. In other words, the entwined wire-like deposits observed for EC:DMC case have no resemblance to those that have grown out of the early stage electrodeposits (Figure 1C [i]), whereas the smooth morphology observed in the FEC:G2 case retains the spatial uniformity in electrodeposit morphology observed at lower capacities (Figure 1C [l]). The degree of morphological uniformity increases across the electrolyte spectrum, as shown in Figure 4 (a–d). The chemical composition of the SEI after cycling (100 cycles) is examined via XPS survey spectra (Figure S2) along with high-resolution C 1s and Li 1s spectra (Figure S5; Tables S2 and S3). The results are briefly summarized and contrasted with those of lower capacity (0.05 mAh/cm^2, early stage of deposition) in Figures 4B and 4C. Similar to the lower-capacity case, the F:C and F:O ratios increase about 200%, with an increase in ethylene -C-C-/C-H linkage (from 32.12% to 57.46%) and decrease in ethylene oxide C-C-O (from 40.22% to 28.76%) and Li_2CO_3 (from 27.67% to 13.78%) across the range of electrolyte chemistries (EC:DMC to FEC:G2), as shown in Figures 4B and 4C. The LiF:Li_2CO_3 ratio increases about ~700% across the electrolyte spectrum. This suggests that the chemical composition of the fluorine-enriched polyene SEI formed at lower capacities is retained during the cycling of electrodeposited Li. The cleaning action of G2 dissolving the oxygen-rich carbonaceous species at the interface lasts throughout the cycle life, further preserving the fluorine-enriched interface.

EIS performed on plated/stripped Li (1 mA/cm^2, 1 mAh/cm^2) on SS for the set of electrolyte compositions (EC:DMC to FEC:G2) is shown in Figure S6. The impedance loops in Nyquist plots are relatively smaller than that of lower capacity (i.e., compare

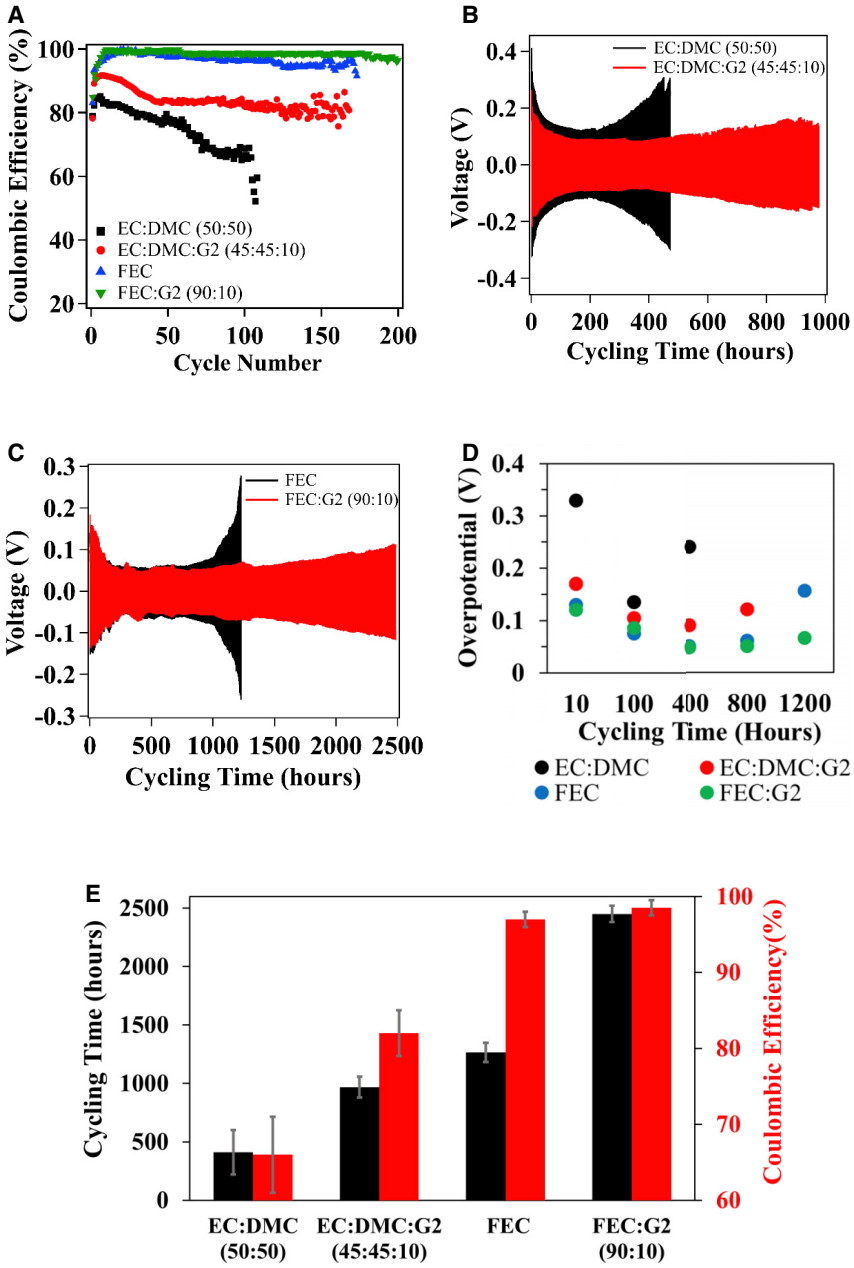

Figure 6. Reversibility and cyclability of Li electrodeposits formed under the influence of electrolytes of different chemistries

(A) CE of electrodeposited Li on polished stainless steel (Li||SS) for a maximum of 200 cycles at 1 mA/cm^2 and 1 mAh/cm^2.

(B) Shown is the galvanostatic plating/stripping voltage profile of the symmetric Li anode (Li||Li) at a current density of 1 mA/cm^2 and capacity of 1 mAh/cm^2 in EC:DMC and EC:DMC:G2.

(C) Shown is the galvanostatic plating/stripping voltage profile of the symmetric Li anode (Li||Li) at a current density of 1 mA/cm^2 and capacity of 1 mAh/cm^2 in FEC and FEC:G2.

(D) Nucleation overpotential of different electrolytes at different cycling hours.

(E) Plot of symmetric cell cycling time and CE (at 100 cycles) for an average of 4 coin cells. The error bars represent the standard deviation of the data. The electrolytes are EC:DMC (50:50), EC:DMC:G2 (45:45:10), FEC, and FEC:G2 (90:10), each containing 1M $LiPF_6$ salt.

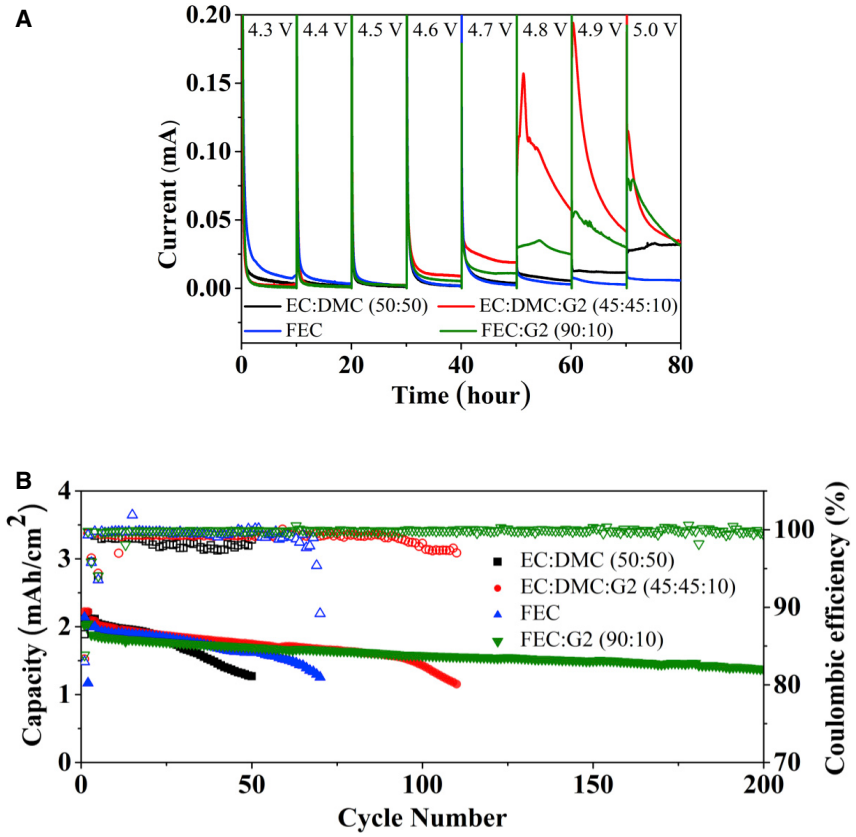

Figure 7. Oxidative stability and electrochemical performance of electrolytes in Li||NCM622 cells with a thin Li anode (50 μm) and NCM622 cathode (2 mAh/cm^2)

(A) Electrochemical floating test of different electrolytes in Li||NCM622 cells.

(B and C) Discharge capacity retention and CE over 200 cycles for Li||NCM cells with a thin Li anode (50 μm) and NCM622 cathode (2 mAh/cm^2). The cells are cycled in (B) CC-CV charge mode (constant current of 0.5C–4.2 V and constant voltage until the current decreases to 0.2) and (C) CC discharge mode at 0.5C. 1C=(2 mA/cm^2). The electrolytes are EC:DMC (50:50), EC:DMC:G2 (45:45:10), FEC, and FEC:G2 (90:10), each containing 1M $LiPF_6$ salt.

the Nyquist plots in Figure S6A with Figure 3A), which indicates lower SEI and CT resistance for electrodeposits of Li cycled at higher capacity. Consistent with our previous observations, the FEC:G2 case shows the lowest SEI and CT resistance of all electrolytes (Figure S6B). A study of energy barriers to Li ion movement at the interface can aid our understanding of underlying transport-reaction kinetics of the SEI formed by different electrolytes. To this end, we performed temperature-dependent impedance spectroscopy of Li electrodeposits formed on SS at lower capacity (0.05 mAh/cm^2) and after 100 cycle capacity (1 mAh/cm^2). The resulting SEI and CT resistances (R) are fitted to the Arrhenius equation,[35] $k = {}^{1}/_{R} = A\exp(-Ea/_{RT})$, where k (1/s) is the rate constant, A (1/s) is the pre-exponential factor, Ea (J/mol) is the activation energy, R (8.314 J/[mol K]) is the gas constant, and T (K) is the temperature, as shown in Figure S7. The calculated activation energy, Ea, and pre-exponential factor, $ln(A)$, are presented in Figure 5 and Table S6. The activation energy of SEI and CT kinetics follows a decreasing trend across the set of electrolytes at all capacities of electrodeposition/cycling (0.05 mAh/cm^2, 100 cycles); e.g., the Ea of the SEI at 0.05 mAh/cm^2 is 52.42 kJ/mol (EC:DMC), 47.61 kJ/mol (EC:DMC:G2), 38.95 kJ/mol (FEC), and 37.01 kJ/mol (FEC:G2). Small changes in activation energy can produce considerable effects on the kinetics because Ea is

scaled exponentially in the Arrhenius equation. Cycling at higher capacities increases the activation energy; i.e., *Ea* of 100 cycles > 0.05 mAh/cm^2. However, the *Ea* of SEI and CT kinetics is quite similar across 0.05 mAh/cm^2 and 100 cycles for FEC:G2 (i.e., at 0.05 mAh/cm^2, the *Ea* is 37.01 kJ/mol [SEI] and 37.99 kJ/mol [CT] compared with 38.12 kJ/mol [SEI] and 38.99 kJ/mol [CT] at 100 cycles), in contrast with the large difference seen in the case of EC:DMC (i.e., at 0.05 mAh/cm^2, the *Ea* is 52.42 kJ/mol [SEI] and 56.26 kJ/mol [CT] compared with 59.64 kJ/mol [SEI] and 63.87 kJ/mol [CT] at 100 cycles). Similarly, the *Ea* of SEI and CT kinetics is more similar across 0.05 mAh/cm^2 and 100 cycles for the G2-added one than the base electrolyte (i.e., compare EC:DMC:G2 and EC:DMC or FEC:G2 and FEC), as shown in Figure 5. This can be rationalized as follows. The fluorine-enriched polyene SEI (FEC:G2) having higher *Ds* and exchange current, and chemically preserved through the plating/stripping cycles (as observed previously), shows similar activation energies across the capacities. The effect of G2 on cleaning the interphase is crucial in preserving the kinetics across the cycling life of Li metal. Fairly similar observations can be made from the trend of the pre-exponential factor ($ln(A)$) across the set of electrolytes, as shown in Table S6. The $ln(A)$ decreases across the set of electrolytes at all stages of deposition; i.e., at 0.05 mAh/cm^2, $ln(A)$ of the SEI kinetics of EC:DMC is 16.4 compared with 10.6 of FEC:G2. The pre-exponential factor A is related to the entropy of activation for first-order kinetics by the transition state theory[36–38] as $A = \frac{k_B T e}{h} \exp\left(\Delta S/R\right)$, where k_B (1.38 × 10^{-23} J/K) is the Boltzmann constant, T (K) is the temperature, e is 2.72, h (6.62 × 10^{-34} m^2 kg/s) is the Planck constant, ΔS (J/K) is the change in entropy of activation, and R (8.314 J/(mol K)) is the gas constant. The calculated ΔS is negative for all electrolytes, as shown in Table S6, suggesting that the entropy decreases during the transport-reaction kinetics at the interphase. The decreasing trend of $ln(A)$ observed previously results in a larger negative ΔS across the set of electrolytes; e.g., the FEC:G2 electrolyte shows the largest negative ΔS of any electrolytes (−165.1 J/K [SEI] and −174.1 J/K [CT] at 0.05 mAh/cm^2), which indicates that the ionic motions in its interphase are less random (i.e., more correlated) than other electrolytes. Comparing across the capacities (i.e., 0.05 mAh/cm^2 and 100 cycles), each electrolyte shows an increase in ΔS, quite like the increase in *Ea* observed previously; e.g., ΔS of SEI kinetics changes from −116.8 J/K at 0.05 mAh/cm^2 to −85.2 J/K at 100 cycles for the EC:DMC electrolyte. Therefore, we reason that the interphase of all electrolytes shows signs of impeding kinetics and more randomized motion of Li ions with the progression of plating/stripping cycles.

Reversibility and cyclability of Li electrodeposits

The electrochemical reversibility and cyclability of Li electrodeposits under the influence of the different electrolytes is shown in Figure 6. CE tests performed in electrochemical cells (Li||SS) at a current density of 1 mA/cm^2 and capacity of 1 mAh/cm^2 (Figure 6A) corroborate the previous inferences. The CE increases across the set of electrolytes; i.e., at 100 cycles, the CE follows the order EC:DMC (66.7%) < EC:DMC:G2 (81.2%) < FEC (96.5%) < FEC:G2 (98.8%). The G2-added fluorinated electrolyte (FEC:G2) shows a consistent CE of 97%–99.5% through its cycle life up to 200 cycles, in contrast to the oscillating/drastically dropping CE of other electrolytes; e.g., the CE of the regular carbonate electrolyte oscillates between 64% and 70% around 80–100 cycles before drastically dropping to below 55% toward the end of its cycle life. Although CE is widely used to assess the electrochemical reversibility of metals in asymmetric cells (e.g., Li||SS), the information obtained from it about the dendritic growth of Li metal and its effect on cycle life is rather limited. In other words, different tests are needed to evaluate the interaction of the Li anode with the electrolyte-separator membrane during cycling in perpetuating

short-circuiting of the cell. To this end, we performed galvanostatic plating/stripping experiments of Li anodes in symmetric cells (Li||Li) under the influence of different electrolytes at a similar current density of 1 mA/cm^2 and capacity of 1 mAh/cm^2. The resulting voltage profiles over the cycle life of cells are shown in Figures 6B and 6C and elaborated (plotted in time intervals) in Figure S8. Two observations can be easily made. First, the G2 additive enhances the cycle life (time to short circuit) of the base electrolyte by almost 2-fold; i.e., comparing EC:DMC (470 h) with EC:DMC:G2 (980 h) or FEC (1,230 h) with FEC:G2 (2,480 h). Also, the cycle life increases across the spectrum of electrolytes. Second, the voltage window of cycling is lower for the G2-added electrolytes compared with the base electrolytes, and the voltage window decreases across the electrolytes. The voltage window is also arch shaped (U shape), with higher voltages recorded during initial cycles, followed by a plateau during intermediate cycles, and another increase in voltage toward the end of the cycle life. This is elaborated in Figure 6D. The voltage (overpotential) is recorded at the beginning of plating cycles for different electrolytes at different times of the cycle life. The arch shape of the voltage and the decrease in voltage window across all electrolytes is even more apparent; e.g., considering the EC:DMC case, the potentials are 0.329, 0.135, and 0.24 V at 10, 100, and 400 cycles, respectively. We speculate that the arch shape is a result of (1) higher overpotentials of plating during the initial cycling stage because of the ion transport resistance offered by the existing native SEI on the Li anode; followed by (2) the plateau region, most likely because of facile ion transport through the newly formed SEI; and (3) a subsequent increase in overpotential toward the end of the cycle life because of increased resistance to ion transport, a result of thickening SEI formed by degradation products of electrolyte and dead Li in repeated plating/stripping.[39–41] The lowest overpotential and longest voltage plateau shown by FEC:G2 electrolyte proves the efficacy of a preserved fluorine-enriched SEI in promoting long-lasting ion transport. The CE and galvanostatic stripping/plating cycle life evaluated over four coin cells are summarized in Figure 6E. The EC:DMC case shows bigger error bars of CE and cycle life in contrast to other electrolytes because of the uncertainty of reversibility and cell failure in the carbonate electrolyte lacking advantages of a facile SEI.

These observations can be summarized as follows. The chemical composition and enhanced surface energetics (i.e., decreased activation energy for Li^+ diffusion and reaction) of the fluorine-enriched SEI formed by FEC:G2 electrolyte is preserved through repeated stripping/plating of the Li metal anode. The modified SEI enables lower polarization and uniform plating of Li metal, mitigating the chemical and morphological instabilities of the Li metal-electrolyte interphase and enhancing the reversibility and cycle life of the Li metal anode.

Performance of LMBs

The suitability of the electrolytes in LMBs is evaluated by performing voltammetry, floating tests, and full-cell electrochemical cycling tests, as shown in Figures S9 and 7. Linear scan voltammetry performed at scan rates of 2 mV/s and up to 6.5 V show oxidation (i.e., higher current) of all electrolytes above 5 V (Figure S9). A strong oxidation peak is observed around 5.7–5.8 V for the carbonate electrolytes with and without G2 (EC:DMC and EC:DMC:G2), indicating that the regular carbonates (EC:DMC) have lower oxidative stability compared with fluorinated ones (FEC).[10,42,43] A more rigorous test of oxidative stability is the floating test, where the electrolytes are subjected to long time steps (10 h) of increasing potential (4.3–5 V) in Li||NCM cells to study the evolution of current (leakage current), as shown in Figure 7A. All electrolytes show oxidative stability below 4.5 V. The leakage currents increase across all electrolytes above 4.5 V and are strikingly high for the

Please cite this article in press as: Biswal et al., A reaction-dissolution strategy for designing solid electrolyte interphases with stable energetics for lithium metal anodes, Cell Reports Physical Science (2022), https://doi.org/10.1016/j.xcrp.2022.100948

G2-added ones (EC:DMC:G2 and FEC:G2), conceivably because of low oxidative stability of G2.[44] The results of the two aforementioned procedures establish the voltage range of operation for the electrolytes to be below 4.5 V in an LMB.

The electrochemical performance of the electrolytes is evaluated in LMBs containing a thin Li (50 μm) anode paired against an NCM 622 cathode of areal capacity of 2 mAh/cm^2. The cells are cycled in CC-CV charge mode (constant current of 0.5 C–4.2 V and constant voltage until the current decreases to 0.2 C) and CC discharge mode at 0.5 C. The resulting charge discharge voltage profiles are shown in Figure S10, and the CE and discharge capacity retention profile are summarized in Figure 7B. The FEC:G2 case shows the highest average CE of 99.85% (5–200 cycles) and discharge capacity retention of 74% (compared with the fifth cycle) after 200 cycles. The EC:DMC, EC:DMC:G2, and FEC electrolytes show considerably lower CE and discharge capacity retention. The CE and discharge capacity retention of EC:DMC:G2 is greater than that of the FEC-only case. This measurement is in clear contrast to the previously conducted CE study in Li||SS cells (Figure 6A) and oxidative stability studies in Figures S9 and 7A. We envisage that the discrepancy is likely due to beneficial action of the G2 in a carbonate-rich environment on the cathode electrolyte interface (CEI) of the NCM cathode. Additional studies are necessary to deconvolute the effect of such ether additives on transitional metal cathodes of LMBs. Overall, the electrochemical performance of LMBs is significantly improved by utilization of G2-enriched fluorinated electrolytes.

We studied the role of carbonate and fluorinated electrolytes with and without ethers as additives on the morphology, chemical composition, interfacial energetics, and electrochemical reversibility of Li anodes during early stages of electrodeposition as well as later stages of deep cycling of the Li anode. Aptly designed experiments shed light on the role of surface energetics (transport-reaction kinetics) of the SEI at different stages of cycle life of Li electrodeposits. The chemical nature of the SEI is deliberately manipulated via electrolytes of contrasting chemistries (carbonate versus fluorinated) to study the physicochemical nature of Li electrodeposition. The transport-reaction kinetics of the SEI are shown to play an important role in Li plating and can be modulated by rational choice of electrolyte components. We demonstrated that incorporation of an ether-based additive (G2) has a beneficial "cleaning" effect on Li electroplating and is necessary for preserving the surface energetics (transport-reaction kinetics), chemical nature, and uniform morphology observed at initial stages of electroplating through deep cycling of the Li anode. Finally, the electrolyte chemistry (ether-enriched fluorinated electrolyte) is shown to have superior electrochemical performance in an LMB. Designing and preserving interfaces with enhanced transport-reaction kinetics is a feasible solution to stabilize electrodeposition of reactive metals such as Li. Systematic studies of electrolytes with different ratios of carbonate and ether components are necessary to enable and optimize the reaction-dissolution strategy for Li metal anodes. Additional studies dealing with the fundamental approach of understanding and eliminating morphological and chemical instabilities at the initiation step of dendrite nucleation for reactive metal electrodeposition are paramount to accelerate the realization of high-energy-density, high-performance, reactive metal batteries.

EXPERIMENTAL PROCEDURES

Resource availability

Lead contact

Further information and requests for the resources are available from the lead contact, Lynden A. Archer (laa25@cornell.edu).

Materials availability

This study did not generate unique materials.

Data and code availability

All data supporting the findings of this study are available within the article and are described in the supplemental information or are available from the lead contact upon reasonable request.

SUPPLEMENTAL INFORMATION

Supplemental information can be found online at https://doi.org/10.1016/j.xcrp.2022.100948.

ACKNOWLEDGMENTS

The research was supported as part of the Center for Mesoscale Transport Properties, an Energy Frontier Research Center supported by the Department of Energy (DOE), Office of Science, Basic Energy Sciences, under award DE-SC0012673. The electron microscopy facilities made use of the Cornell Center for Materials Research Shared Facilities, which are supported through the NSF MRSEC program (DMR-1719875). The interface characterization work made use of the facilities available in CESI, Cornell.

AUTHOR CONTRIBUTIONS

Conceptualization, P.B. and L.A.A.; methodology, P.B., J.R., A.K., Y.D., Q.Z., J.Y., and L.A.A.; formal analysis, P.B. and A.K.; investigation, P.B., J.R., A.K., Y.D., Q.Z., and J.Y.; writing – original draft, P.B. and L.A.A.; writing – review and editing, P.B. and L.A.A.; resources, J.Y.; supervision, L.A.A.; funding acquisition, L.A.A.

DECLARATION OF INTERESTS

The authors declare no competing interests.

Received: December 9, 2021
Revised: February 24, 2022
Accepted: May 27, 2022
Published: June 21, 2022

REFERENCES

1. Aurbach, D. (2000). Review of selected electrode–solution interactions which determine the performance of Li and Li ion batteries. J. Power Sources *89*, 206–218. https://doi.org/10.1016/s0378-7753(00)00431-6.

2. Zachman, M.J., Tu, Z., Choudhury, S., Archer, L.A., and Kourkoutis, L.F. (2018). Cryo-STEM mapping of solid–liquid interfaces and dendrites in lithium-metal batteries. Nature *560*, 345–349. https://doi.org/10.1038/s41586-018-0397-3.

3. Tikekar, M.D., Choudhury, S., Tu, Z., and Archer, L.A. (2016). Design principles for electrolytes and interfaces for stable lithium-metal batteries. Nat. Energy *1*, 16114. https://doi.org/10.1038/nenergy.2016.114.

4. Biswal, P., Stalin, S., Kludze, A., Choudhury, S., and Archer, L.A. (2019). Nucleation and early stage growth of Li electrodeposits. Nano Lett. *19*, 8191–8200. https://doi.org/10.1021/acs.nanolett.9b03548.

5. Wood, K.N., Kazyak, E., Chadwick, A.F., Chen, K.H., Zhang, J.G., Thornton, K., and Dasgupta, N.P. (2016). Dendrites and pits: untangling the complex behavior of lithium metal anodes through operando video microscopy. ACS Cent. Sci. *2*, 790–801. https://doi.org/10.1021/acscentsci.6b00260.

6. Shi, F., Pei, A., Boyle, D.T., Xie, J., Yu, X., Zhang, X., and Cui, Y. (2018). Lithium metal stripping beneath the solid electrolyte interphase. Proc. Natl. Acad. Sci. U S A *115*, 8529–8534. https://doi.org/10.1073/pnas.1806878115.

7. Zheng, J., Kim, M.S., Tu, Z., Choudhury, S., Tang, T., and Archer, L.A. (2020). Regulating electrodeposition morphology of lithium: towards commercially relevant secondary Li metal batteries. Chem. Soc. Rev. *49*, 2701–2750. https://doi.org/10.1039/c9cs00883g.

8. Miao, R., Yang, J., Feng, X., Jia, H., Wang, J., and Nuli, Y. (2014). Novel dual-salts electrolyte solution for dendrite-free lithium-metal based rechargeable batteries with high cycle reversibility. J. Power Sources *271*, 291–297. https://doi.org/10.1016/j.jpowsour.2014.08.011.

9. Qian, J., Henderson, W.A., Xu, W., Bhattacharya, P., Engelhard, M., Borodin, O., and Zhang, J.G. (2015). High rate and stable cycling of lithium metal anode. Nat. Commun. *6*, 6362. https://doi.org/10.1038/ncomms7362.

10. Suo, L., Xue, W., Gobet, M., Greenbaum, S.G., Wang, C., Chen, Y., Yang, W., Li, Y., and Li, J. (2018). Fluorine-donating electrolytes enable highly reversible 5-V-class Li metal batteries. Proc. Natl. Acad. Sci. U S A *115*, 1156–1161. https://doi.org/10.1073/pnas.1712895115.

11. Gordin, M.L., Dai, F., Chen, S., Xu, T., Song, J., Tang, D., Azimi, N., Zhang, Z., and Wang, D.

(2014). Bis (2, 2, 2-trifluoroethyl) ether as an electrolyte co-solvent for mitigating self-discharge in lithium–sulfur batteries. ACS Appl. Mater. Interfaces *6*, 8006–8010. https://doi.org/10.1021/am501665s.

12. Aurbach, D., Pollak, E., Elazari, R., Salitra, G., Kelley, C.S., and Affinito, J. (2009). On the surface chemical aspects of very high energy density, rechargeable Li–sulfur batteries. J. Electrochem. Soc. *156*, A694. https://doi.org/10.1149/1.3148721.

13. Kim, H., Wu, F., Lee, J.T., Nitta, N., Lin, H.T., Oschatz, M., Cho, W.I., Kaskel, S., Borodin, O., and Yushin, G. (2015). In situ formation of protective coatings on sulfur cathodes in lithium batteries with LiFSI-based organic electrolytes. Adv. Energy Mater. *5*, 1401792. https://doi.org/10.1002/aenm.201401792.

14. Choudhury, S. (2019). Lithium fluoride additives for stable cycling of lithium batteries at high current densities. In Rational Design of Nanostructured Polymer Electrolytes and Solid–Liquid Interphases for Lithium Batteries (Springer), pp. 81–94.

15. Lu, Y., Tu, Z., Shu, J., and Archer, L.A. (2015). Stable lithium electrodeposition in salt-reinforced electrolytes. J. Power Sources *279*, 413–418. https://doi.org/10.1016/j.jpowsour.2015.01.030.

16. Zhang, X.Q., Cheng, X.B., Chen, X., Yan, C., and Zhang, Q. (2017). Fluoroethylene carbonate additives to render uniform Li deposits in lithium metal batteries. Adv. Funct. Mater. *27*, 1605989. https://doi.org/10.1002/adfm.201605989.

17. Choudhury, S., Wei, S., Ozhabes, Y., Gunceler, D., Zachman, M.J., Tu, Z., Shin, J.H., Nath, P., Agrawal, A., Kourkoutis, L.F., et al. (2017). Designing solid-liquid interphases for sodium batteries. Nat. Commun. *8*, 898. https://doi.org/10.1038/s41467-017-00742-x.

18. Biswal, P., Kludze, A., Rodrigues, J., Deng, Y., Moon, T., Stalin, S., Zhao, Q., Yin, J., Kourkoutis, L.F., and Archer, L.A. (2021). The early-stage growth and reversibility of Li electrodeposition in Br-rich electrolytes. Proc. Natl. Acad. Sci. U S A *118*. e2012071118. https://doi.org/10.1073/pnas.2012071118.

19. Suo, L., Hu, Y.S., Li, H., Armand, M., and Chen, L. (2013). A new class of solvent-in-salt electrolyte for high-energy rechargeable metallic lithium batteries. Nat. Commun. *4*, 1481. https://doi.org/10.1038/ncomms2513.

20. Yamada, Y., Wang, J., Ko, S., Watanabe, E., and Yamada, A. (2019). Advances and issues in developing salt-concentrated battery electrolytes. Nat. Energy *4*, 269–280. https://doi.org/10.1038/s41560-019-0336-z.

21. Markevich, E., Salitra, G., Chesneau, F., Schmidt, M., and Aurbach, D. (2017). Very stable lithium metal stripping–plating at a high rate and high areal capacity in fluoroethylene carbonate-based organic electrolyte solution. ACS Energy Lett. *2*, 1321–1326. https://doi.org/10.1021/acsenergylett.7b00300.

22. Hou, T., Fong, K.D., Wang, J., and Persson, K.A. (2021). The solvation structure, transport properties and reduction behavior of carbonate-based electrolytes of lithium-ion batteries. Chem. Sci. *12*, 14740–14751. https://doi.org/10.1039/d1sc04265c.

23. Zhang, X.Q., Li, T., Li, B.Q., Zhang, R., Shi, P., Yan, C., Huang, J., and Zhang, Q. (2020). A sustainable solid electrolyte interphase for high-energy-density lithium metal batteries under practical conditions. Angew. Chem. *132*, 3278–3283. https://doi.org/10.1002/ange.201911724.

24. Zhang, Z., Hu, L., Wu, H., Weng, W., Koh, M., Redfern, P.C., Curtiss, L.A., and Amine, K. (2013). Fluorinated electrolytes for 5 V lithium-ion battery chemistry. Energy Environ. Sci. *6*, 1806. https://doi.org/10.1039/c3ee24414h.

25. Tang, S., and Zhao, H. (2014). Glymes as versatile solvents for chemical reactions and processes: from the laboratory to industry. RSC Adv. *4*, 11251. https://doi.org/10.1039/c3ra47191h.

26. Wang, A., Kadam, S., Li, H., Shi, S., and Qi, Y. (2018). Review on modeling of the anode solid electrolyte interphase (SEI) for lithium-ion batteries. NPJ Comput. Mater. *4*, 15. https://doi.org/10.1038/s41524-018-0064-0.

27. Delp, S.A., Borodin, O., Olguin, M., Eisner, C.G., Allen, J.L., and Jow, T.R. (2016). Importance of reduction and oxidation stability of high voltage electrolytes and additives. Electrochim. Acta *209*, 498–510. https://doi.org/10.1016/j.electacta.2016.05.100.

28. Westman, K., Dugas, R., Jankowski, P., Wieczorek, W., Gachot, G., Morcrette, M., Irisarri, E., Ponrouch, A., Palacín, M.R., Tarascon, J.M., and Johansson, P. (2018). Diglyme based electrolytes for sodium-ion batteries. ACS Appl. Energy Mater. *1*, 2671–2680. https://doi.org/10.1021/acsaem.8b00360.

29. Markevich, E., Salitra, G., and Aurbach, D. (2017). Fluoroethylene carbonate as an important component for the formation of an effective solid electrolyte interphase on anodes and cathodes for advanced Li-ion batteries. ACS Energy Lett. *2*, 1337–1345. https://doi.org/10.1021/acsenergylett.7b00163.

30. Markevich, E., Salitra, G., Hartmann, P., Kulisch, J., Aurbach, D., Park, K.J., Yoon, C.S., and Sun, Y.K. (2019). New insights related to rechargeable lithium batteries: Li metal anodes, Ni rich LiNixCoyMnzO2 cathodes and beyond them. J. Electrochem. Soc. *166*, A5265–A5274. https://doi.org/10.1149/2.0261903jes.

31. Jin, Y., Kneusels, N.J.H., Marbella, L.E., Castillo-Martínez, E., Magusin, P.C.M.M., Weatherup, R.S., Jónsson, E., Liu, T., Paul, S., and Grey, C.P. (2018). Understanding fluoroethylene carbonate and vinylene carbonate-based electrolytes for Si anodes in lithium ion batteries with NMR spectroscopy. J. Am. Chem. Soc. *140*, 9854–9867. https://doi.org/10.1021/jacs.8b03408.

32. Benitez, L., and Seminario, J.M. (2017). Ion diffusivity through the solid electrolyte interphase in lithium-ion batteries. J. Electrochem. Soc. *164*, E3159–E3170. https://doi.org/10.1149/2.0181711jes.

33. Guan, P., Liu, L., and Lin, X. (2015). Simulation and experiment on solid electrolyte interphase (SEI) morphology evolution and lithium-ion diffusion. J. Electrochem. Soc. *162*, A1798–A1808. https://doi.org/10.1149/2.0521509jes.

34. Yildirim, H., Kinaci, A., Chan, M.K.Y., and Greeley, J.P. (2015). First-principles analysis of defect thermodynamics and ion transport in inorganic SEI compounds: LiF and NaF. ACS Appl. Mater. Interfaces *7*, 18985–18996. https://doi.org/10.1021/acsami.5b02904.

35. Arrhenius, S. (1889). Über die Reaktionsgeschwindigkeit bei der Inversion von Rohrzucker durch Säuren. Z. Phys. Chem. *4U*, 226–248. https://doi.org/10.1515/zpch-1889-0416.

36. Frost, A.A., and Pearson, R.G. (1971). Kinetics and Mechanism (Wiley Eastern, First reprint), p. 7.

37. Glasstone, S., Laidler, K.J., and Eyring, H. (1941). The theory of Rate Processes; the Kinetics of Chemical Reactions, Viscosity, Diffusion, and Electrochemical Phenomena (No. 541.39) (McGraw-Hill Book Company).

38. Sanjeev, R., A Padmavathi, D., and Jagannadham, V. (2018). The 'yard stick'to interpret the entropy of activation in chemical kinetics: a physical–organic chemistry exercise. World J. Chem. Ed. *6*, 78–81. https://doi.org/10.12691/wjce-6-1-12.

39. Chen, K.H., Wood, K.N., Kazyak, E., LePage, W.S., Davis, A.L., Sanchez, A.J., and Dasgupta, N.P. (2017). Dead lithium: mass transport effects on voltage, capacity, and failure of lithium metal anodes. J. Mater. Chem. *5*, 11671–11681. https://doi.org/10.1039/c7ta00371d.

40. Lu, Y., Gu, S., Hong, X., Rui, K., Huang, X., Jin, J., Chen, C., Yang, J., and Wen, Z. (2018). Pre-modified Li3PS4 based interphase for lithium anode towards high-performance Li-S battery. Energy Storage Mater. *11*, 16–23. https://doi.org/10.1016/j.ensm.2017.09.007.

41. Xia, S., Lopez, J., Liang, C., Zhang, Z., Bao, Z., Cui, Y., and Liu, W. (2019). High-rate and large-capacity lithium metal anode enabled by volume conformal and self-healable composite polymer electrolyte. Adv. Sci. *6*, 1802353. https://doi.org/10.1002/advs.201802353.

42. He, M., Su, C.C., Peebles, C., and Zhang, Z. (2021). The impact of different substituents in fluorinated cyclic carbonates in the performance of high voltage lithium-ion battery electrolyte. J. Electrochem. Soc. *168*, 010505. https://doi.org/10.1149/1945-7111/abd44b.

43. Fan, X., Chen, L., Borodin, O., Ji, X., Chen, J., Hou, S., Deng, T., Zheng, J., Yang, C., Liou, S.C., et al. (2018). Non-flammable electrolyte enables Li-metal batteries with aggressive cathode chemistries. Nat. Nanotechnol. *13*, 715–722. https://doi.org/10.1038/s41565-018-0183-2.

44. Choudhury, S., Tu, Z., Nijamudheen, A., Zachman, M.J., Stalin, S., Deng, Y., Zhao, Q., Vu, D., Kourkoutis, L.F., Mendoza-Cortes, J.L., and Archer, L.A. (2019). Stabilizing polymer electrolytes in high-voltage lithium batteries. Nat. Commun. *10*, 3091. https://doi.org/10.1038/s41467-019-11015-0.